Title

Determining the static electronic and vibrational energy correlations via twodimensional electronic-vibrational spectroscopy

Authors

Dong, Hui
Lewis, Nicholas HC
Oliver, Thomas AA
et al.

Publication Date

2015

DOI

10.1063/1.4919684

Peer reviewed

Determining the static electronic and vibrational energy correlations via two-dimensional electronic-vibrational spectroscopy

Hui Dong,[1,2,3] Nicholas H. C. Lewis,[1,2,3] Thomas A. A. Oliver,[1,2,3] and Graham R. Fleming[1,2,3,a)]

[1)] *Department of Chemistry, University of California, Berkeley, CA 94720*

[2)] *Physical Biosciences Division, Lawrence Berkeley National Laboratory, Berkeley, CA, 94720*

[3)] *Kavli Energy NanoSciences Institute at the University of California, Berkeley and the Lawrence Berkeley National Laboratory, Berkeley, CA 94720*

Changes in the electronic structure of pigments in protein environments and of polar molecules in solution inevitably induces a re-adaption of molecular nuclear structure. Both changes of electronic and vibrational energies can be probed with visible or infrared lasers, such as two-dimensional electronic or vibrational spectroscopies. The extent to which the two changes are correlated remains elusive. The recent demonstration of two-dimensional electronic-vibrational (2DEV) spectroscopy potentially enables a direct measurement of this correlation experimentally. However, it has hitherto been unclear how to characterize the correlation from the spectra. In this paper, we present a theoretical formalism to demonstrate the slope of the nodal line between the excited state absorption and ground state bleach peaks in the spectra as a characterization of the correlation between electronic and vibrational transition energies. We also show the dynamics of the nodal line slope is correlated to the vibrational spectral dynamics. Additionally, we demonstrate the fundamental 2DEV spectral line-shape of a monomer with newly developed response functions.

[a)] Electronic mail: grfleming@lbl.gov

I. INTRODUCTION

Energy and charge transfer steps are critical in many light-initiated processes in both natural and artificial systems. Recently, an increasing number of experimental studies suggested the possibility of active engagement of molecular vibrational excited states in charge separation[1–3]. In a pump-push experiment on organic photo-voltaic cells, *Bakulin et. al.* showed[4] a clear relative photocurrent increase after an infrared (IR) push pulse. A later experiment[3] demonstrated a delicate control of the ratio between charge separation and charge recombination via mode-specific IR excitation of vibrations. However, the physical role of these vibrational effects is not entirely clear from both experimental and theoretical perspectives. The recently developed two-dimensional electronic-vibrational spectroscopy[5] provides a direct frequency-resolved probe of the vibrational dynamics upon photon-induced electronic excitation. The potential applications of this new spectroscopic method have not been fully explored, and detailed theoretical investigations are required, in parallel with further experimental developments, to elucidate the specific information available.

One of the potential application of 2DEV spectroscopy is to probe the correlation between electronic and vibrational energies for solute molecules in solution and for chromophores in proteins. It is well know that the electronic structure of a molecule is modified by its local environment compared to its corresponding properties in gas phase[6–8]. In biological systems, this modification is critically important in terms of regulating the optical properties of individual pigments to optimize the functional design of photo-initiated process[4,9,10]. One primary example is the tuning of the chromophores' absorption spectra in light-harvesting complexes[11]. The protein environment modifies the electronic transition energy to capture a broad part of the solar spectrum[11]. The change of the electronic structure inevitably induces a distortion of the potential energy surface, which, in turn, results in a variation of the molecular structures. Theoretically, the impact of the electronic distortion is captured by an effective adiabatic Born-Oppenheimer potential[12,13], which guides the motion of nuclei.

The change of nuclear configuration can be incisively probed by a variety of infrared laser related spectroscopic methods. For example, two-dimensional infrared spectroscopy (2DIR)[14] is employed to study vibrational frequency changes and the associated spectral dynamics[15,16] on the electronic ground state. Changes of the electronic transition energy can also be probed via two-dimensional electronic spectroscopy (2DES)[17–21]. However, the

connection between the changes of the two transition energies has remained elusive, due to the lack of incisive experimental detection methods. 2DEV fills this gap by combining the advantages of 2DIR and 2DES methods. Upon excitation with a laser pulse pair resonant with an electronic transition, molecules are prepared on the electronically excited or ground state with the nuclear motions perturbed. After a waiting time, a infrared laser pulse subsequently probes the response of the nuclear motions. The dynamics embedded in signal during the waiting time reflects the nuclear reorganization, or the protein configuration re-adaption upon the electronic excitation.

Although the vibrational frequencies are known to be affected by the change of electronic state, it is not yet entirely clear how the vibrational frequency is correlated to the electronic energy shift in a specific environment. Interpretation of 2DEV spectroscopy opens a window towards understanding the correlation between the electronic and vibrational degrees of freedom. This paper is devoted to revealing the signatures of a static correlation in 2DEV spectra with newly developed response functions. The study of dynamical correlation is presented in a forthcoming paper[22]. We describe a model based on monomers with one explicit vibrational mode and derive the corresponding response functions. The spectra in the time-domain and the frequency-domain are illustrated following the theoretical calculation. We then demonstrate the connection between the nodal line[23–28] slope and the correlation strength between electronic and vibrational transition energies by showing the corresponding spectra for different correlation strengths. We also discuss the meaning of "rephasing" and nonrephasing pulses sequences for an experiment involving two different types of optical transitions.

II. MODEL

To demonstrate the physical principles involved, we first apply the theoretical formalism to a minimal model of monomers with one coupled harmonic vibrational mode. The potential energy surfaces of the ground state $|g\rangle$ and excited state $|e\rangle$ are shown as parabolic curves in Figure 1(a). The potential energy surface of excited state is displaced relatively to that of the ground state. To account for the change of the excited state potential, we assume a frequency shift, namely, $\omega_e \neq \omega_g$. The first two lowest vibrational levels on both the electronic ground and excited states are illustrated in Figure 1(a) as (0,1) and (0', 1')

respectively. In the 2DEV experiment, the first two laser pulses excite the electronic levels. A IR pulse probes the nuclear response of the prepared system upon the change of electronic degree of freedom (DoF). If the first two laser pulses have insufficient energy to excite one quanta of the probed vibrational mode, only the $0 \to 0'$ transition with energy ϵ_{eg} is active. Taking this into consideration, we further simplify the system to 4 levels, as shown in Figure 1(a). The Hamiltonian of the system is given by,

$$\begin{aligned} H = & H_{g0} \left|g0\right\rangle \left\langle g0\right| + \left(\hbar\omega_g + H_{g1}\right) \left|g1\right\rangle \left\langle g1\right| \\ & + \left(\epsilon_{eg} + H_{e0'}\right) \left|e0'\right\rangle \left\langle e0'\right| \\ & + \left(\epsilon_{eg} + \hbar\omega_e + H_{e1'}\right) \left|e1'\right\rangle \left\langle e1'\right|, \end{aligned} \tag{1}$$

where

$$H_{g0} = \sum_{\xi} \hbar\omega_{\xi} a_{\xi}^{\dagger} a_{\xi} + \sum_{j} \hbar\nu_j b_j^{\dagger} b_j, \tag{2}$$

$$H_{g1} = \sum_{\xi} \hbar\omega_{\xi} a_{\xi}^{\dagger} a_{\xi} + \sum_{j} \hbar\nu_j [b_j^{\dagger} b_j + h_j (b_j^{\dagger} + b_j)], \tag{3}$$

$$\begin{aligned} H_{e0'} = & \sum_{\xi} \hbar\omega_{\xi} [a_{\xi}^{\dagger} a_{\xi} + d_{\xi} (a_{\xi}^{\dagger} + a_{\xi})] \\ & + \sum_{j} \hbar\nu_j [b_j^{\dagger} b_j + \alpha_0 h_j (b_j^{\dagger} + b_j)], \end{aligned} \tag{4}$$

$$\begin{aligned} H_{e1'} = & \sum_{\xi} \hbar\omega_{\xi} [a_{\xi}^{\dagger} a_{\xi} + d_{\xi} (a_{\xi}^{\dagger} + a_{\xi})] \\ & + \sum_{j} \hbar\nu_j [b_j^{\dagger} b_j + \alpha_1 h_j (b_j^{\dagger} + b_j)]. \end{aligned} \tag{5}$$

Here, a_{ξ} and b_j are the environmental DoF (bath) annihilation operators for the electronic and vibrational transitions respectively. The dynamics of the environmental DoFs results in dynamical changes of both electronic and vibrational transition energies[29,30]. d_{ξ} and h_j are the corresponding displacements of environmental DoFs for the electronic and vibrational modes. The direct parameters to characterize these couplings to the environments are the spectral densities $\mathcal{J}_e(\omega) = \sum_{\xi} d_{\xi}^2 \omega_{\xi}^2 \delta(\omega - \omega_{\xi})$ and $\mathcal{J}_v(\omega) = \sum_j h_j^2 \nu_j^2 \delta(\omega - \omega_j)$ for the electronic and vibrational DoFs. The total displacement is given by the reorganization energy $\lambda_i = \int d\omega \mathcal{J}_i(\omega)/\omega$, $(i = e, v)$. In the current paper, we use independent environment for the electronic and vibrational transitions, noting the different response timescales, which implies the coupling to different portions of the environmental DoFs. However, this assumption does not exclude the possibility of correlated fluctuation between the electronic and vibrational

transition energies, due to correlation through the effective Born-Oppenheimer potential[12,13]. The response of the system with correlated fluctuation will be discussed elsewhere.

The parameters α_0 and α_1 characterize the relative coupling strengths of the $v = 0'$ and $v = 1'$ states respectively to their environment, compared to the coupling strength of $v = 1$ state to its environment. In terms of the spectral density, the two parameters provide a scaling of reorganization energies. In the following discussion, we assume the coupling of vibrational mode to the bath on the electronically excited state is not significantly altered from its counterpart on the electronic ground state. Typically, we will choose $0 < \alpha_0 < 1$ and $\alpha_1 > 1$ in the following simulation. Experimentally, the two parameters can be extracted from the measurement of the central line slope[22] in 2DEV and transient-2DIR[31,32]. In the current model, we only consider the dephasing of the vibrational mode, and neglect the relaxation between vibrational states.

Beside the dynamic fluctuations of the transition energies, the stationary configuration differences in pigment-protein complexes and the chromophore-solvent induce a static variance of both electronic and vibrational transition energies among molecules. The interaction energy between the molecule and its environment can be described as a polarizable molecule in an electrostatic potential, ϕ, formed by the surrounding molecules. A perturbation term $H_p(\phi)$ is assumed in the total molecular Hamiltonian to account for this interaction. With the Rayleigh-Schrdinger perturbation theory, one can obtain a correction to the electronic energy $E_n(Q, \phi)$, where Q is the nuclear coordinate. The change of electronic energy, in turn, induces an effective potential $V_{\text{eff}}(Q, \phi)$. In terms of the vibrational frequency, this change can be generally written[12,13] as $\Delta\omega = \omega(\phi) - \omega'$, where $\omega(\phi)$ and ω' are the vibrational frequencies in solution and gas phase respectively. This disorder is the so-called inhomogeneous broadening. To simplify the discussion but retaining a physical picture, we will consider the correlation between electronic and vibrational energies, by assuming the inhomogeneous broadening of both electronic and vibrational DoF is described by a joint two-dimensional Gaussian distribution,

$$p(\epsilon_{eg}, \omega_g) = \frac{\exp\{-[\frac{\left(\epsilon_{eg}-\epsilon^0_{eg}\right)^2}{\sigma^2_{eg}} + \frac{\left(\omega_g-\omega^0_g\right)^2}{\sigma^2_{\omega g}} - 2\zeta\frac{\left(\epsilon_{eg}-\epsilon^0_{eg}\right)\left(\omega_g-\omega^0_g\right)}{\sigma_{eg}\sigma_{\omega_g}}]/[2\left(1-\zeta^2\right)]\}}{2\pi\sigma_{eg}\sigma_{\omega_g}\sqrt{1-\zeta^2}}. \tag{6}$$

Here, σ_{eg} and σ_{ω_g} are the widths of the distributions of electronic and vibrational transition energies, and ϵ^0_{eg} and ω^0_g are the mean electronic and vibrational transition energies in the

condensed phase, respectively. The correlation strength between the two transition energies is characterized by a coefficient ζ ($-1 \leq \zeta \leq 1$). The coefficient in different regions is defined as follows[23],

$$\begin{cases} \zeta = 0 & \text{No correlation,} \\ 0 < \zeta \leq 1 & \text{Positive Correlation,} \\ -1 \leq \zeta < 0 & \text{Negative Correlation.} \end{cases} \tag{7}$$

In Figures 1(b-g), we show three types of correlations with the joint distributions of electronic (ϵ_{eg}) and vibrational (ω_g) transition energies in the right panel. Figure 1(b) shows the uncorrelated case ($\zeta = 0$) with a horizontal distribution. The change of the electronic transition energy has no effect on the shape of the vibrational potential. Figure 1(c) describes a slanted distribution for the positively correlated case. A disorder of the increasing the electronic transition energy compared to the mean frequencies $\left(\epsilon_{eg}^0, \omega_g^0\right)$, is associated with an increases the vibrational transition frequencies ω_g, or vice versa. Figure 1(d) shows the distribution of the two transition energies for a negatively correlated case, where an increase of electronic transition energy is associated with a decreased vibrational transition energy. The changes of potential energy surfaces on both the electronic ground and excited state could potentially be different. However, to simplify the following discussion, we assume the frequency of vibrational mode on the excited state is only different from the ground state one with a constant, $\delta\omega = \omega_g - \omega_e$.

III. RESULTS AND DISCUSSIONS

The non-linear spectroscopic signals can be calculated with the response function formalism[33]. These response functions for 2DES and 2DIR have been presented and used to calculate the corresponding spectra[8,14]. In these experiments, the pump and probe pulses address the same type of transitions. For example, in 2DES experiments, the optical response is detected via the electronic transition after the pump with the electronic transition dipole. However, the 2DEV method involves a pump through an electronic transition, and a different probe via vibrational transition. In Figure 2, we show four response pathways with double-sided Feynman diagrams, which can be divided into two groups: rephasing (a,b) and nonrephasing (c,d). For the rephasing pathways in 2DES and 2DIR, the phase of the

polarization during the first coherence period (t_1) is the complex conjugate of that during the second coherence time (t_3). The disorder induced phase differences between molecules are removed during the second coherence time when $t_3 = t_1$. Due to two different types of transitions for the two coherence time t_1 and t_3, the accumulated phase $\Phi = \epsilon_{eg} t_1 - \omega_g t_3$ is not completely removed in 2DEV spectroscopy. In Figure 3, we show the distribution of trajectories in the phase space for three correlation strengths $\zeta = 0$ and ± 1. In the simulation, we use the parameters, $\epsilon^0_{eg} = 12200\text{cm}^{-1}$, $\omega_{g0} = 1410\text{cm}^{-1}$ and $\omega_{e0} = 1460\text{cm}^{-1}$. The disorder of the site energy and vibrational DoF are $\sigma_{eg} = 400\text{cm}^{-1}$ and $\sigma_{\omega_g} = 10\text{cm}^{-1}$. The distribution of electronic and vibrational transition energies are presented in Figures 3(a, c, e). The phase differences between molecules are shown as the width of the beam in Figures 3(b, d, f). The color indicates the relative density of trajectories at specific time. For the uncorrelated case, $\zeta = 0$ in Figure 3(a), phase evolution during the detection time t_3 is not correlated with that during the first waiting time t_1. And the trajectories are not refocused, illustrated as a lens-like diagram in Figure 3(b). For this case, the rephasing pathway has no "echo-like" feature, as is typical in the rephasing sequence of 2DES and 2DIR spectroscopies[14,21]. However, we still adapt this terminology of rephasing following the previous studies. For positive correlation $\zeta > 0$, with an extreme case ($\zeta = 1$) shown in Figure 3(c), the phase recovery speed is positively proportional to that in the first waiting time t_1. The trajectories are refocused at $t_3 = \epsilon^0_{eg} t_1/\omega^0_g$. Under this circumstance, an echo appears with the removal of the phase inhomogeneity during the evolution of different molecules. An interesting case is negative correlation $\zeta < 0$, with the extreme case ($\zeta = -1$) shown in Figure 3(e). The divergence of the beam during the detecting time t_3 implies a strong impact of inhomogeneity on the signal strength. In following discussion, we will demonstrate how to distinguish the three cases through line-shape of 2DEV spectrum.

The response functions of the rephasing pathways of excited state absorption (ESA) and ground state bleach (GSB) can be calculated using the second order cumulant expansion[33]:

$$R_e^{\mathrm{R}}(t_1,t_2,t_3) = -\left\langle \mu_{eg}^2 \mu_{1'0'}^2 \right\rangle \exp\begin{bmatrix} -g_e^*(t_1) + i\epsilon_{eg}t_1 - i\omega_e t_3 \\ -g_v^*(t_1)\,\alpha_0^2 + g_v(t_2)\,\alpha_0(\alpha_1-\alpha_0) - g_v(t_3)\,(\alpha_1-\alpha_0)^2 \\ -g_v^*(t_1+t_2)\,\alpha_0(\alpha_1-\alpha_0) - g_v(t_2+t_3)\,\alpha_0(\alpha_1-\alpha_0) \\ +g_v^*(t_1+t_2+t_3)\,\alpha_0(\alpha_1-\alpha_0) \end{bmatrix} \quad (8)$$

$$R_g^{\mathrm{R}}(t_1,t_2,t_3) = \left\langle \mu_{eg}^2 \mu_{10}^2 \right\rangle \exp\begin{bmatrix} -g_e^*(t_1) + i\epsilon_{eg}t_1 - i\omega_g t_3 \\ -g_v^*(t_1)\,\alpha_0^2 + g_v^*(t_2)\,\alpha_0 - g_v(t_3) - g_v^*(t_1+t_2)\,\alpha_0 \\ -g_v^*(t_2+t_3)\,\alpha_0 + g_v^*(t_1+t_2+t_3)\,\alpha_0 \end{bmatrix}, \quad (9)$$

where $g_e(t)$ and $g_v(t)$ are the corresponding line broadening functions for the electronic and vibrational DoF, and μ_{eg} and μ_{10} ($\mu_{1'0'}$) are the corresponding electronic transition dipole and vibrational transition $0 \to 1$ ($0' \to 1'$) dipole. The line broadening function is given by

$$g_i(t) = \int d\omega \frac{\mathcal{J}_i(\omega)}{\omega^2}[(1-\cos\omega t)\coth(\beta\omega/2) + i(\sin\omega t - \omega t)], \quad (10)$$

where $\beta = 1/(kT)$ is the inverse temperature. In the following discussion, we perform all simulations at $T = 77$K with the Drude-Lorentian spectral density for electronic DoF

$$\mathcal{J}_e(\omega) = \frac{2\lambda\omega_c\omega}{\omega_c^2+\omega^2}, \quad (11)$$

with reorganization energy $\lambda = 50\,\mathrm{cm}^{-1}$ and cutoff frequency $\omega_c = 50\,\mathrm{cm}^{-1}$. For the vibrational mode, we use Kubo line broadening function[14],

$$g_v(t) = (\Delta\omega\tau_c)^2\left[e^{-t/\tau_c} + \frac{t}{\tau_c} - 1\right]. \quad (12)$$

Here, we use typical parameters: fluctuation amplitude $\Delta\omega = 50\mathrm{cm}^{-1}$ and inverse correlation time $1/\tau_c = 10\mathrm{cm}^{-1}$ for the bath of the vibrational mode. A more general model for the vibrational mode would be a Brownian oscillator. In high temperature limit $k_BT \gg 1/\tau_c$, we use Kubo lineshape to simplify the numerical calculation. One drawback of this approximation is that the temperature dependence is not explicitly shown, although it can be added through the fluctuation amplitude $\Delta\omega \sim T^{1/2}$.

Figures 4 (a,b) show the time domain signal (absolute value) of the rephasing pathways for systems with correlation strengths $\zeta = 0$ (a) and $\zeta = 1.0$ (b). In this simulation, we use the same parameters as that in Figure3 and assume the same vibrational transition dipole strength on the ground and excited states. Figure 4(a) shows a decay of the signal over the first coherence time t_1 for the uncorrelated case $\zeta = 0$. Once correlation is assumed ($\zeta = 1.0$), the signal shows a clear echo-like feature with a t_1-dependent peak position along

the second coherence time t_3 in Figure 4(b). This observation reflects the discussion about echo formation in the previous section. The frequency domain spectrum is generated by the Fourier transformation of the time-domain signal. In the following discussion, we simplify the calculation by assuming the impulsive limit, where the pulse duration is much shorter than any of the dynamical time scales of the system. Discussion on the signal with finite-width pulse in time domain involves the convolution of laser spectrum and response functions, and goes beyond the current scope of reproducing basic lineshape in 2DEV spectra. For the impulsive limit, the frequency-domain spectrum is equivalent to the Fourier transformation of the response functions with respect to the coherence time t_1 and t_3,

$$S^{\mathrm{R}}(\omega_1, t_2, \omega_3) = \mathrm{FFT}[R_e^R(t_1, t_2, t_3) + R_g^R(t_1, t_2, t_3)]. \tag{13}$$

In Figure 4, we also show the frequency-domain line-shape of the real (c,d), imaginary (e,f) part, and absolute value (g,h) of the rephasing signal for correlation strengths $\zeta = 0$ and $\zeta = 1.0$, respectively. Both ESA and GSB features, with opposite signs, are illustrated as the double peaks at bottom $(\epsilon_{eg}, \omega_{e0})$ and top $(\epsilon_{eg}, \omega_{g0})$ respectively in the real spectra.

Because of the correlation through the phase factor $\exp[i\epsilon_{eg}t_1 - i\omega_e t_3]$, the line-shape of the peaks are twisted along a line with a slope $k' = \omega_e/\epsilon_{eg}$ in both the real and imaginary spectra, shown in Figures 4 (c-f). This trivial slope obscures the aforementioned correlation between the electronic and vibrational transition energy. The absolute value spectra remove the trivial correlation in the phase term $\exp[i\epsilon_{eg}t_1 - i\omega_e t_3]$, however, they lose the relative sign of the peaks, which are hard to distinguish if the line-broadening of the vibrational levels is large compared to the separation of the ground and excited state vibrational frequencies, see Figures 4(g, h). On the other hand, Fourier spectra of the rephasing signals contain contributions from both absorptive and dispersive parts for each axis (ω_1 and ω_3)[14]. The pure dispersive part decays slowly with respect to the deviation from the central frequency and broadens the peak with consequent loss of detailed structure. One way of enhancing the resolution of spectrum[14] is to eliminate the contribution from the dispersive part by adding the rephasing part with a inverted sign of ω_1 to the spectrum of the nonrephasing pathways, which are illustrated in Figures 2(c-d). The pure absorptive spectrum $S^{\mathrm{abp}}(\omega_1, t_2, \omega_3)$ is defined as

$$S^{\mathrm{abp}}(\omega_1, t_2, \omega_3) = \mathrm{Re}\left[S^{\mathrm{R}}(-\omega_1, t_2, \omega_3) + S^{\mathrm{NR}}(\omega_1, t_2, \omega_3)\right], \tag{14}$$

where $S^{\mathrm{NR}}(\omega_1, t_2, \omega_3) = \mathrm{FFT}[R_e^{NR}(t_1, t_2, t_3) + R_g^{NR}(t_1, t_2, t_3)]$ is the Fourier transformed

spectrum of the nonrephasing signals. The response functions of the nonrephasing pathways can be calculated with a similar method to that used for rephasing pathways,

$$R_e^{\mathrm{NR}}(t_1,t_2,t_3) = -\left\langle \mu_{eg}^2 \mu_{1'0'}^2 \right\rangle \exp\left[-g_e(t_1) - i\epsilon_{eg}t_1 - i\omega_e t_3\right] \times \exp\begin{bmatrix} -g_v(t_1)\,\alpha_0^2 - g_v^*(t_2)\,\alpha_0(\alpha_1-\alpha_0) - g_v(t_3)\,(\alpha_1-\alpha_0)^2 \\ +g_v(t_1+t_2)\,\alpha_0(\alpha_1-\alpha_0) + g_v^*(t_2+t_3)\,\alpha_0(\alpha_1-\alpha_0) \\ -g_v(t_1+t_2+t_3)\,\alpha_0(\alpha_1-\alpha_0) \end{bmatrix}, \quad (15)$$

$$R_g^{\mathrm{NR}}(t_1,t_2,t_3) = \left\langle \mu_{eg}^2 \mu_{10}^2 \right\rangle \exp\left[-g_e(t_1) - i\epsilon_{eg}t_1 - i\omega_g t_3\right] \times \exp\begin{bmatrix} -g_v(t_1)\,\alpha_0^2 - g_v(t_2)\,\alpha_0 - g_v(t_3) + g_v(t_1+t_2)\,\alpha_0 \\ +g_v(t_2+t_3)\,\alpha_0 - g_v(t_1+t_2+t_3)\,\alpha_0 \end{bmatrix}. \quad (16)$$

In Figures 5(a-d), we show the simulated pure absorptive 2DEV spectra for different waiting time t_2 = 0, 0.5, 1, and 4ps. In the simulation, we use the same parameters as those used in Figure 4 with the correlation coefficient fixed at $\zeta = 1.0$. The ESA and GSB peaks have a clearly reduced width. The nodal line between the two peaks is slanted due to the correlation between the electronic and vibrational transition energies. A positive slope corresponds to the positively correlated case shown in Figure 1(b). The linear fits of the nodal lines at each waiting time are illustrated by black solid lines in Figures 5(a-d), along with the fits from the previous figures to illustrate the change of the nodal line slope. The slope of nodal line decreases with increasing waiting time. We show the dynamical change of the slope in Figure 5(f). The open circles show the numerical simulation results as t_2 increases. The red dashed line shows a fit with a single exponential decay. The fit of the slope decay with single exponential gives a lifetime T_c = 0.56ps, which is similar to the fluctuation correlation time for the vibrational mode, τ_c = 530fs. As shown by the response functions in Eqs. (8,9) and Eqs. (15,16), the dynamics of the line-shape during the waiting time t_2 depends only on the spectral dynamics of vibrational modes. In the model, we assume no relaxation between vibrational states. We also assume the first two laser pulses excite the system to an electronic excited state, while leaving the vibrational degree of freedom on its ground state. Therefore, the inclusion of vibrational relaxation would not affect the dynamics during t_1 and t_2. During the detection time t_3 , the relaxation of the vibrational mode will increase the dephasing time of vibrational mode. Thus, the two peaks will be broaden along ω_3 axis with inclusion of relaxation between vibrational states, if the relaxation between vibrational states is considered.

To quantitatively explore the relation of the nodal line slope to the correlation between the electronic and vibrational transition energies, we plot the pure absorptive spectra for different correlation coefficients $\zeta = -1.0$ (a), -0.5 (b), 0 (c), 0.5(d), and 1.0(e) in Figure 6 at waiting time $t_2 = 0$ps. Figure 6(c) shows an almost horizontal nodal line, which resembles the two dimensional distribution of the electronic and vibrational transition energy shown in Figure1(b). For negative correlation, we see a negative nodal line slope in Figures 6(a,b). The orientation of nodal line slope resembles that of the slanted distribution of the electronic and vibrational transition energy shown in Figure1(d-f). The direct correspondence between the slope and the correlation between electronic and vibrational transition energies enables a qualitative approach to determine the type of the correlation between electronic and vibrational transition energies in different environments.

With the increasing correlation strength, a clear increase of slope of nodal line is shown in Figure 6(a-e). In Figure 6(f), we quantitatively show the nodal line slope as a function of the correlation strength, ζ, at waiting times $t_2 = 0$ps and 4ps. The slope at $t_2 = 0$ps shows the initial correlation between the electronic and vibrational transition energies, while that at $t_2 = 4$ps illustrates the aforementioned residual correlation after partial correlation decays via vibrational spectral diffusion. In Figure 6 (f), the slope displays an asymmetry between the positive and negative correlations at $t_2 = 0$ps, because of the initial correlation in the vibrational mode, which induces a slope for system with no disorder[22]. This asymmetry disappears with vibrational spectral diffusion at longer waiting time, $t_2 = 4$ps. The curves present a clear linear dependence over the correlation strength, ζ, for both the initial value at $t_2 = 0$ps and long-time residual value at $t_2 = 4$ps. The simple linear dependence offers a direct way to detect the correlation strength via measurement of the 2DEV signal.

In the discussion above, the first two laser pulses only create vibrational eigenstates for corresponding vibrational mode within the detected window . However, wave-packets of low-frequency vibrational modes are inevitably generated with broadband laser pulses. The extent to which the wavepacket will affect the line-shape presented needs to be addressed, especially when the frequencies of wavepackets are beyond the infrared detection window. In the following discussion, an additional low frequency vibrational mode is included in the system via

$$H' = H'_{g0} \left|g0\right\rangle \left\langle g0\right| + H'_{g1} \left|g1\right\rangle \left\langle g1\right| + H'_{e0'} \left|e0'\right\rangle \left\langle e0'\right| + H'_{e1'} \left|e1'\right\rangle \left\langle e1'\right|,$$

where $H'_{g0} = H_{g0} + \hbar\omega'_c c^\dagger c$, $H'_{g1} = H_{g1} + \hbar\omega'_c c^\dagger c$, $H'_{e0'} = H_{e0'} + \hbar\omega'_c \left[c^\dagger c + f(c^\dagger + c)\right]$, and $H'_{e1'} = H_{e1'} + \hbar\omega'_c \left[c^\dagger c + f(c^\dagger + c)\right]$. We assume this low-frequency mode has no coupling to the vibrational modes within the detection window. The response functions for rephasing pathways are

$$R_e^{\mathrm{aR}}(t_1, t_2, t_3) = R_e^{\mathrm{R}}(t_1, t_2, t_3) \times F^*(t_1), \tag{17}$$

$$R_g^{\mathrm{aR}}(t_1, t_2, t_3) = R_g^{\mathrm{R}}(t_1, t_2, t_3) \times F^*(t_1), \tag{18}$$

Here $F(t_1)$ is the wavepacket interference term[34], $F(t_1) = \sum_{n=0} e^{-s} s^n/n! e^{-in\omega'_c t_1}$, where $s = f^2/2$ is the Huang-Rhys factor. This term will induce peaks at $\epsilon_{eg} + n\omega_c$ with strength modulated by the corresponding Frank-Condon factor $e^{-s}s^n/n!$. The strength is also further modulated by the optical excitation pulses. However, these additional peaks ($n > 1$) have the same signs as that of the corresponding main peaks with $n = 0$ for the GSB and ESA pathways. This additional term only contributes to the dynamics during first coherence time t_1, without any effect on the dynamics during the waiting time t_2. Therefore, the dynamics of each peak will not reflect this wavepacket interference during waiting time t_2. For the nonrephasing pathway, the response functions are

$$R_e^{\mathrm{aNR}}(t_1, t_2, t_3) = R_e^{\mathrm{NR}}(t_1, t_2, t_3) \times F(t_1), \tag{19}$$

$$R_g^{\mathrm{aNR}}(t_1, t_2, t_3) = R_g^{\mathrm{NR}}(t_1, t_2, t_3) \times F(t_1). \tag{20}$$

The low frequency modes bring additional features in the corresponding spectra. However it is still possible to distinguish the basic features, such as the GSB and ESA signals. Also, all the discussion here is based on assumption of a narrow band excitation pulse on red side of molecular absorption. In a forthcoming paper, we will present the simulated spectra with a broad band laser, where the transition with $|g0\rangle \rightarrow |e1'\rangle$ brings additional features related to anharmonicity on both ground and excited state potential surfaces.

IV. CONCLUDING REMARKS

We have established the relationship between the nodal line slope and the correlation between the electronic and nuclear motion in two dimensional electronic-vibrational spectroscopy. A minimal monomer model with one strongly coupled vibrational mode was explored to demonstrate the basic line-shape of 2DEV spectra. With a response function

formalism for the minimal model, we have quantitatively explored the dynamics of the nodal line slope. Using the nodal line slope, we demonstrated the possibility to obtain the correlation strength between the electronic and vibrational transition energies.

One of the promising applications of 2DEV spectroscopy is to directly monitor the energy transfer between chromophores via the associated the vibrational modes as tags for chromophores in different sites. Upon excitation in the exciton basis with a visible laser, energy transfer to unexcited chromophores enhances the associated ESA peaks corresponding the newly populated chromphores. The high resolution of the infrared axis enables the direct observation of the energy transfer pathway, which was previously reconstructed in 2DES spectra[35]. We will present the study of energy transfer pathways via 2DEV in a forthcoming paper.

ACKNOWLEDGMENTS

HD would like to thank Akihito Ishizaki for helpful discussions. This work was supported by the Director, Office of Science, Office of Basic Energy Sciences, of the USA Department of Energy under contract DE-AC02-05CH11231 and the Division of Chemical Sciences, Geosciences and Biosciences Division, Office of Basic Energy Sciences through grant DE-AC03-76SF000098 (at LBNL and UC Berkeley), and NSF under Contract No. NSF CHE- 1012168 and CHE-1362830.

REFERENCES

[1]A. A. Bakulin, A. Rao, V. G. Pavelyev, P. H. M. van Loosdrecht, M. S. Pshenichnikov, D. Niedzialek, J. Cornil, D. Beljonne, and R. H. Friend, "The Role of Driving Energy and Delocalized States for Charge Separation in Organic Semiconductors." Science **335**, 1340–4 (2012).

[2]F. D. Fuller, J. Pan, A. Gelzinis, V. Butkus, S. S. Senlik, D. E. Wilcox, C. F. Yocum, L. Valkunas, D. Abramavicius, and J. P. Ogilvie, "Vibronic Coherence in Oxygenic Photosynthesis." Nat. Chem. **6**, 706–11 (2014).

[3]M. Delor, P. A. Scattergood, I. V. Sazanovich, A. W. Parker, G. M. Greetham, A. J. H. M. Meijer, M. Towrie, and J. A. Weinstein, "Toward Control of Electron Transfer in

Donor-Acceptor Molecules by Bond-Specific Infrared Excitation," Science **346**, 1492–1495 (2014).

[4]R. E. Blankenship, *Molecular Mechanisms of Photosynthesis* (Blackwell Publishing Limited: London, 2001).

[5]T. A. A. Oliver, N. H. C. Lewis, and G. R. Fleming, "Correlating the motion of electrons and nuclei with two-dimensional electronic-vibrational spectroscopy," Proc. Natl. Acad. Sci. U.S.A. **111**, 10061–10066 (2014), also see corrections on Page 16628.

[6]S. E. Sheppard, "The effects of environment and aggregation on the absorption spectra of dyes," Rev. Mod. Phys. **14**, 303–340 (1942).

[7]W. Liptay, "Electrochromism and solvatochromism," Angewandte Chemie International Edition in English **8**, 177–188 (1969).

[8]M. Cho, "Coherent two-dimensional optical spectroscopy," Chem. Rev. **108**, 1331–1418 (2008).

[9]T. Kobayashi, T. Saito, and H. Ohtani, "Real-time spectroscopy of transition states in bacteriorhodopsin during retinal isomerization," Nature **414**, 531–534 (2001).

[10]D. Polli, P. Altoe, O. Weingart, K. M. Spillane, C. Manzoni, D. Brida, G. Tomasello, G. Orlandi, P. Kukura, R. A. Mathies, M. Garavelli, and G. Cerullo, "Conical intersection dynamics of the primary photoisomerization event in vision," Nature **467**, 440–443 (2010).

[11]G. D. Scholes, G. R. Fleming, A. Olaya-Castro, and R. van Grondelle, "Lessons from nature about solar light harvesting," Nat. Chem. **3**, 763–774 (2011).

[12]M. Cho, "Correlation between electronic and molecular structure distortions and vibrational properties. i. adiabatic approximations," J. Chem. Phys. **118**, 3480–3490 (2003).

[13]S. Ham, J.-H. Kim, H. Lee, and M. Cho, "Correlation between electronic and molecular structure distortions and vibrational properties. ii. amide i modes of nma-nd2o complexes," J. Chem. Phys. **118**, 3491–3498 (2003).

[14]P. Hamm and M. Zanni, *Concepts and Methods of 2D Infrared Spectroscopy* (Cambridge University Press, New York, 2011).

[15]J. Zheng, K. Kwak, J. Asbury, X. Chen, I. R. Piletic, and M. D. Fayer, "Ultrafast dynamics of solute-solvent complexation observed at thermal equilibrium in real time," Science **309**, 1338–1343 (2005).

[16]J. Herbst, K. Heyne, and R. Diller, "Femtosecond infrared spectroscopy of bacteriorhodopsin chromophore isomerization," Science **297**, 822–825 (2002).

[17]D. M. Jonas, "Two-dimensional femtosecond spectroscopy," Ann. Rev. Phys. Chem. **54**, 425–463 (2003).

[18]T. Brixner, T. Mancal, I. V. Stiopkin, and G. R. Fleming, "Phase-stabilized two-dimensional electronic spectroscopy," J. Chem. Phys. **121**, 4221–4236 (2004).

[19]M. Cho, "Coherent two-dimensional optical spectroscopy," Chem. Rev. **108**, 1331–1418 (2008).

[20]N. S. Ginsberg, Y.-C. Cheng, and G. R. Fleming, "Two-dimensional electronic spectroscopy of molecular aggregates," Acc. Chem. Res. **42**, 1352–1363 (2009).

[21]G. S. Schlau-Cohen, A. Ishizaki, and G. R. Fleming, "Two-dimensional electronic spectroscopy and photosynthesis: Fundamentals and applications to photosynthetic light-harvesting," Chem. Phys. **386**, 1 – 22 (2011).

[22]N. H. C. Lewis, H. Dong, A. A. Oliver, Thomas, and G. R. Fleming, "Measuring correlated electronic and vibrational spectral dynamics using line shapes in two-dimensional electronic-vibrational spectroscopy," Submitted to J. Chem. Phys. (2015).

[23]N. Demirdoven, M. Khalil, O. Golonzka, and A. Tokmakoff, "Correlation effects in the two-dimensional vibrational spectroscopy of coupled vibrations," J. Phys. Chem. A **105**, 8025–8030 (2001).

[24]N. Demirdoven, M. Khalil, and A. Tokmakoff, "Correlated vibrational dynamics revealed by two-dimensional infrared spectroscopy," Phys. Rev. Lett. **89**, 237401 (2002).

[25]K. Kwac and M. Cho, "Two-color pump-probe spectroscopies of two- and three-level systems: 2-dimensional line shapes and solvation dynamics," J. Phys. Chem. A **107**, 5903–5912 (2003).

[26]S. T. Roberts, J. J. Loparo, and A. Tokmakoff, "Characterization of spectral diffusion from two-dimensional line shapes," J. Chem. Phys. **125**, 084502 (2006).

[27]K. Kwak, S. Park, I. J. Finkelstein, and M. D. Fayer, "Frequency-frequency correlation functions and apodization in two-dimensional infrared vibrational echo spectroscopy: A new approach," J. Chem. Phys. **127**, 124503 (2007).

[28]K. Kwak, D. E. Rosenfeld, and M. D. Fayer, "Taking apart the two-dimensional infrared vibrational echo spectra: More information and elimination of distortions," J. Chem. Phys. **128**, 204505 (2008).

[29]A. J. Leggett, S. Chakravarty, A. T. Dorsey, M. P. A. Fisher, A. Garg, and W. Zwerger, "Dynamics of the dissipative two-state system," Rev. Mod. Phys. **59**, 1–85 (1987).

[30]A. Nitzan, *Chemical Dynamics in Condensed Phases* (Oxford University Press, New York, 2006).

[31]J. Bredenbeck, J. Helbing, and P. Hamm, "Labeling vibrations by light: Ultrafast transient 2d-ir spectroscopy tracks vibrational modes during photoinduced charge transfer," J. Am. Chem. Soc. **126**, 990–991 (2004).

[32]M. S. Lynch, K. M. Slenkamp, M. Cheng, and M. Khalil, "Coherent Fifth-Order Visible-Infrared Spectroscopies: Ultrafast Nonequilibrium Vibrational Dynamics in Solution," J. Phys. Chem. A **116**, 7023–7032 (2012).

[33]S. Mukamel, *Principles of Nonlinear Optical Spectroscopy* (Oxford University Press, USA, 1995).

[34]N. F. Scherer, R. J. Carlson, A. Matro, M. Du, A. J. Ruggiero, V. Romero-Rochin, J. A. Cina, G. R. Fleming, and S. A. Rice, "Fluorescence-detected wave packet interferometry: Time resolved molecular spectroscopy with sequences of femtosecond phase-locked pulses," J. Chem. Phys. **95**, 1487–1511 (1991).

[35]T. Brixner, J. Stenger, H. M. Vaswani, M. Cho, R. E. Blankenship, and G. R. Fleming, "Two-dimensional spectroscopy of electronic couplings in photosynthesis," Nature **434**, 625–628 (2005).

Figure 1. (Color online) Potential energy surfaces (a) on both the ground $|g\rangle$ and excited state $|e\rangle$ (a) and distributions of the electronic (ϵ_{eg}) and vibrational (ω_g) transition energies for three types of correlations (b-d) . (a) The vertical electronic transition energy is denoted as ϵ_{eg}. The vibrational potential is illustrated as a parabolic curve. For generality, we assume a slight change of the energy surface on excited state, namely $\omega_e \neq \omega_g$. The relevant nuclear vibrational levels on the ground and excited state surface are illustrated in figure (a) as (0, 1) and (0' ,1') respectively. (b-d) The distributions of the static electronic ϵ_{eg} and vibrational $\omega_g(\omega_e)$ transition energy are shown for the cases of no correlation (b), positive correlation (c), and negative correlation (d) with the mean frequencies at $\left(\epsilon_{eg}^0, \omega_g^0\right)$.

Figure 2. (Color online) Double-side Feynman diagrams for rephasing (a-b) and nonrephasing(c-d) pathways. The green and black arrows represent the pulses resonant with electronic transition and infrared pulses. The wavy lines illustrate the output signals. The first two pulses create an excited state population ($|e0'\rangle$) for pathways R_e^N and R_e^{NR}, and a ground state population ($|g0\rangle$) for pathways R_g^N and R_g^{NR} . The delay times between pulses are shown on the left.

Figure 4. (Color online) Rephasing signal: absolute value of signal in the time domain (a, b); real part (c,d), imaginary part (e,f), and absolute value (g,h) of signal in the frequency domain. In the simulation, we chose the parameters: $\epsilon_{eg}^0 = 12200\text{cm}^{-1}$, $\omega_g^0 = 1410\text{cm}^{-1}$ and $\omega_e^0 = 1460\text{cm}^{-1}$. The disorder of the electronic and vibrational transitions are $\sigma_{eg} = 400\text{cm}^{-1}$ and $\sigma_{\omega_g} = 10\text{cm}^{-1}$. Here, we assume the correlation coefficient $\zeta = 1.0$. The spectra show the basic line-shape in a 2DEV experiment.

Figure 3. (Color online) Distributions of electronic and vibrational transition energies (a, c, e), and distribution of trajectories (b, d, f) in phase space for three correlation strengths $\zeta = 0$, and ± 1. The transition energies are generated according to the joint Gaussian distribution in Eq.(6). The mean electronic and vibrational transition energies are set, $\epsilon_{eg}^0 = 12200\text{cm}^{-1}$ and $\omega_g^0 = 1410\text{cm}^{-1}$ respectively. The disorder of the electronic and vibrational transition are $\sigma_{eg} = 400\text{cm}^{-1}$ and $\sigma_{\omega_g} = 10\text{cm}^{-1}$. The time delay is in units of 300fs in the figure.

Figure 5. (Color online) Pure absorption 2DEV spectra (a-d) calculated from Eq. 14 and the dynamics of the nodal line slope (e). In the simulation, we used the parameters: $\epsilon_{eg}^0 = 12200\text{cm}^{-1}$, $\omega_g^0 = 1410\text{cm}^{-1}$ and $\omega_e^0 = 1460\text{cm}^{-1}$. The disorder of the site energy and vibrational DoF are $\sigma_{eg} = 400\text{cm}^{-1}$ and $\sigma_{\omega_g} = 10\text{cm}^{-1}$. Here, we assume the correlation coefficient $\zeta = 1.0$. In the spectra, we plot the linear fits of the nodal line at each waiting time as black solid line in figures (a-d). To show the dynamical change in each figure, we also plot the linear fits of nodal line in each previous figure as blue dashed line. The dynamical change of nodal line is plotted as open circles in (e). A single exponential fit gives a lifetime of 560fs, which is similar to the fluctuation correlation time $\tau_c = 530\text{fs}$ for the vibrational mode in the simulation.

Figure 6. (Color online) Line-shape of pure absorptive 2DEV spectra for correlation strengths, (a) $\zeta = -1.0$, (b) $\zeta = -0.5$, (c) $\zeta = 0$, (d) $\zeta = 0.5$, and (e) $\zeta = 1.0$ at a waiting time $t_2 = 0\text{ps}$. (f) The dependence of the nodal line slope as the correlation strength ζ for waiting times $t_2 = 0\text{ps}$ and 4ps. Figures (a-e) qualitatively show that the sign of the slope directly reflects the sign of the correlation coefficient. Figure (f) shows a linear dependence of nodal line slope on the correlation strength ζ.

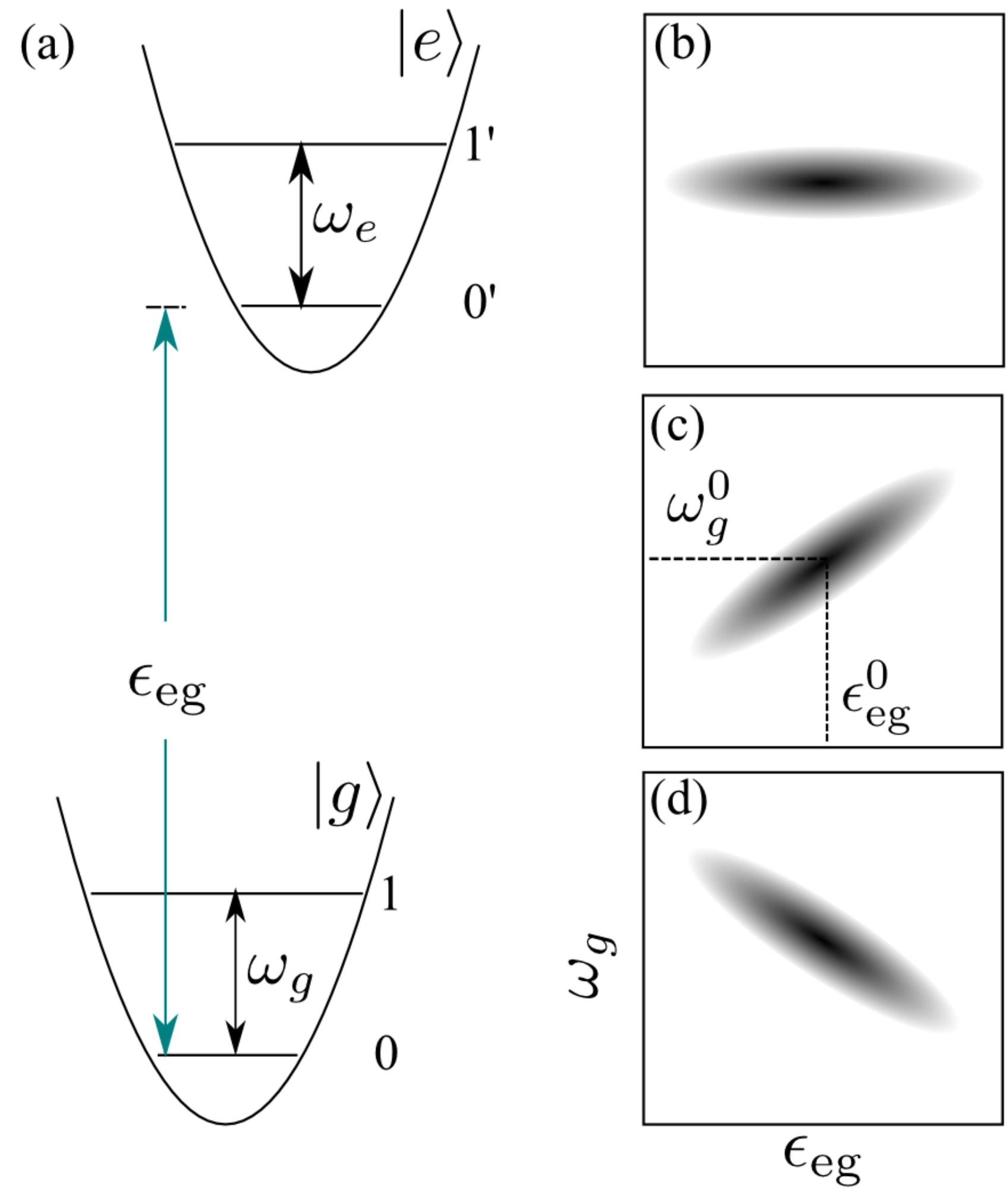
(a)
$|e\rangle$
1'
ω_e
0'
ϵ_{eg}
$|g\rangle$
1
ω_g
0
(b)
(c)
ω_g^0
ϵ_{eg}^0
(d)
ω_g
ϵ_{eg}

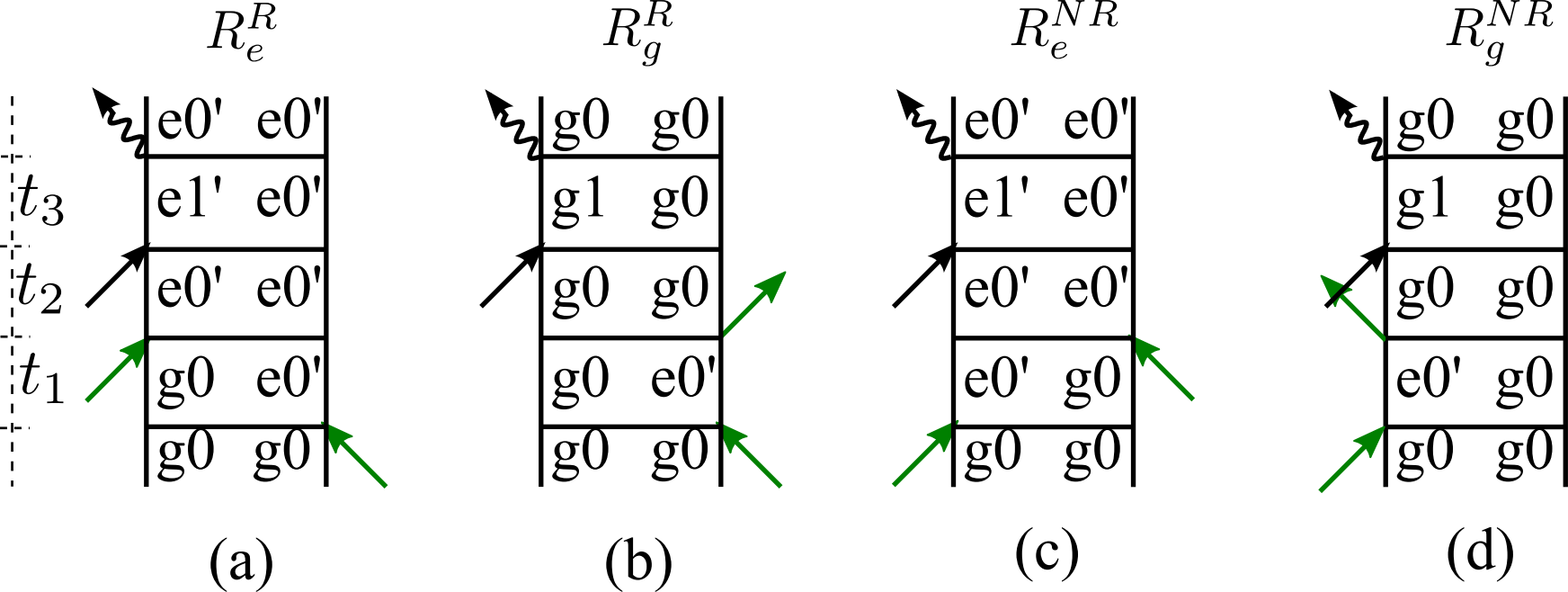
R_e^R
R_g^R
R_e^{NR}
R_g^{NR}
t_3
t_2
t_1
e0' e0'
e1' e0'
e0' e0'
g0 e0'
g0 g0
g0 g0
g1 g0
g0 g0
g0 e0'
g0 g0
e0' e0'
e1' e0'
e0' e0'
e0' g0
g0 g0
g0 g0
g1 g0
g0 g0
e0' g0
g0 g0
(a)
(b)
(c)
(d)

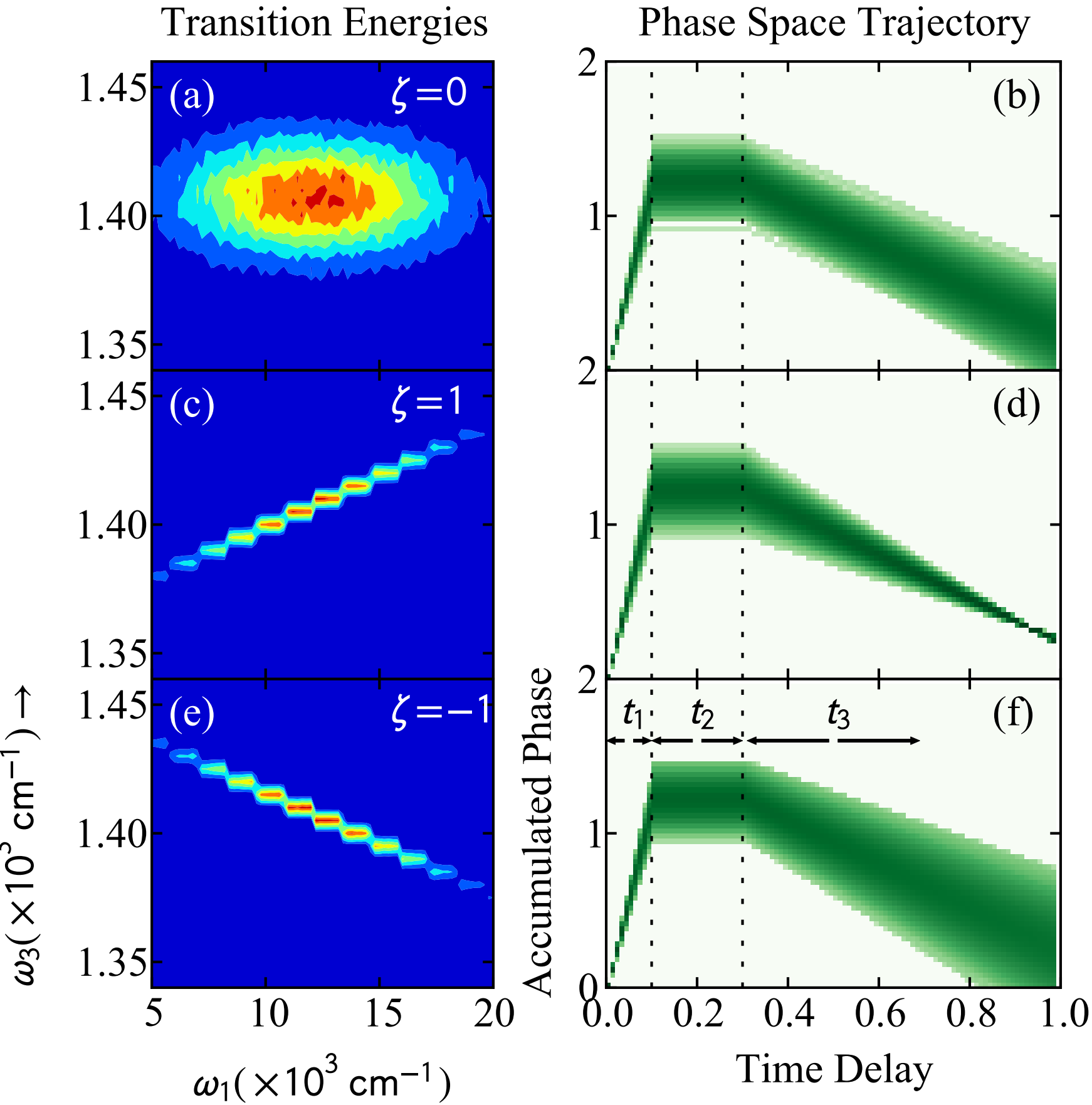
Transition Energies
Phase Space Trajectory
(a)
ζ=0
(c)
ζ=1
(e)
ζ=−1
(b)
(d)
(f)
1.45
1.40
1.35
2
1
0
5
10
15
20
0.0
0.2
0.4
0.6
0.8
1.0
t1
t2
t3
ω3(×10^3 cm^−1) →
ω1(×10^3 cm^−1)
Accumulated Phase
Time Delay

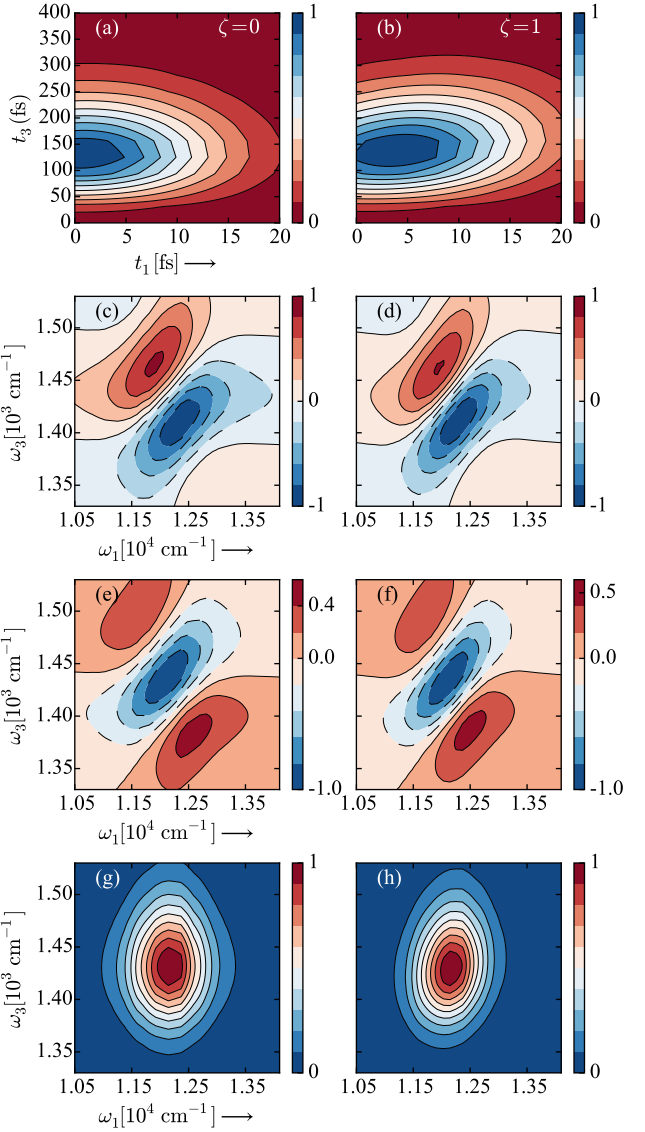
(a)
$\zeta = 0$
(b)
$\zeta = 1$
t_3 (fs)
t_1 [fs] ⟶
(c)
(d)
(e)
(f)
(g)
(h)
$\omega_3[10^3\ \mathrm{cm}^{-1}]$
$\omega_1[10^4\ \mathrm{cm}^{-1}]$ ⟶

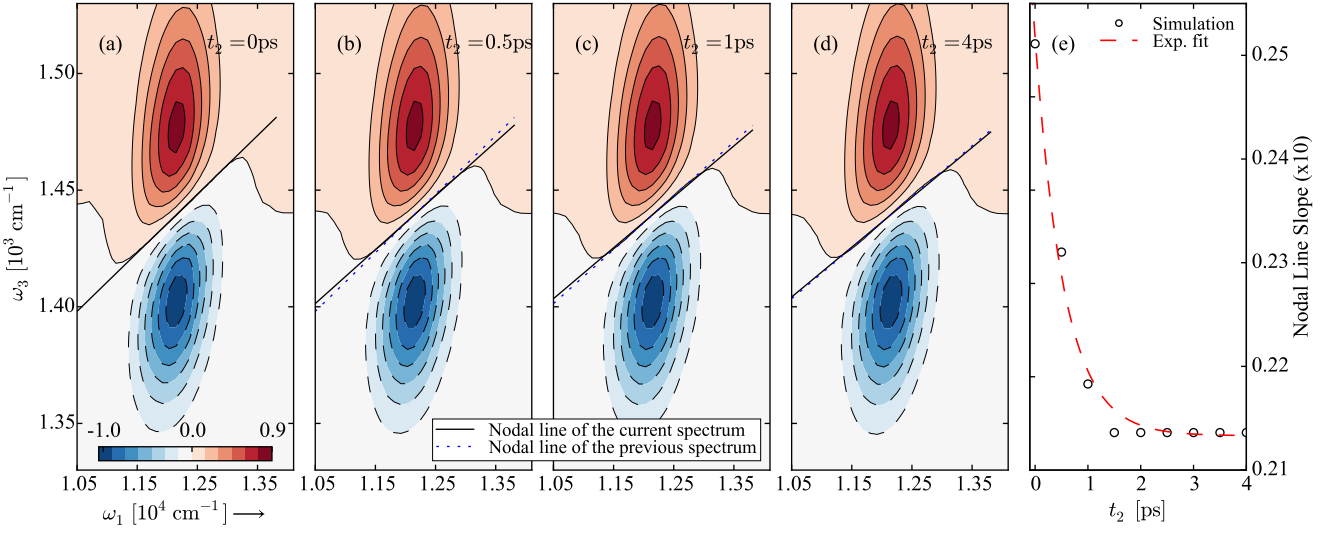
(a)
t_2 =0ps
(b)
t_2 =0.5ps
(c)
t_2 =1ps
(d)
t_2 =4ps
(e)
Simulation
Exp. fit
Nodal Line Slope (x10)
ω_3 [10^3 cm^{-1}]
ω_1 [10^4 cm^{-1}] ⟶
t_2 [ps]
-1.0
0.0
0.9
Nodal line of the current spectrum
Nodal line of the previous spectrum

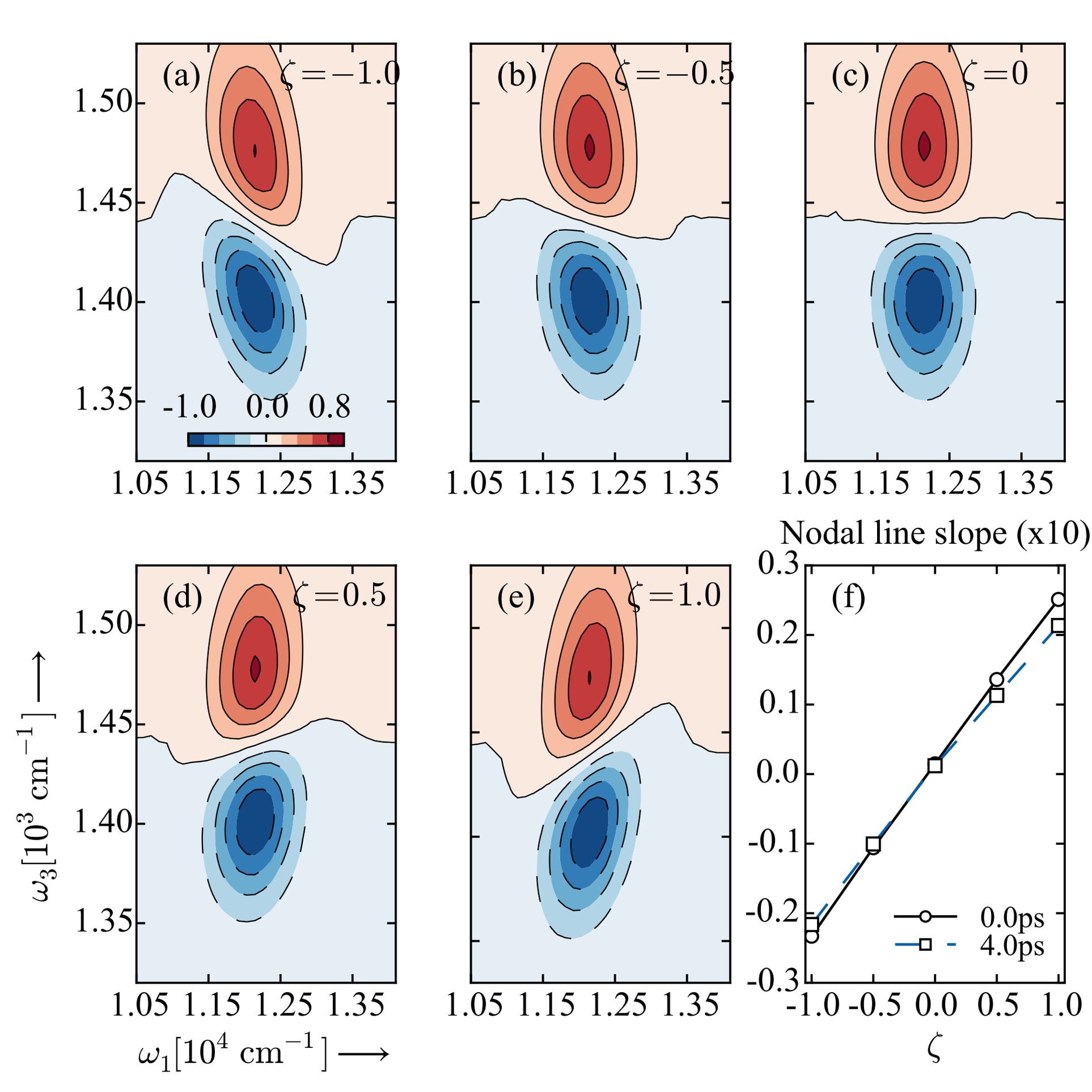
(a) ζ = −1.0
(b) ζ = −0.5
(c) ζ = 0
(d) ζ = 0.5
(e) ζ = 1.0
(f)
-1.0 0.0 0.8
1.50
1.45
1.40
1.35
1.05 1.15 1.25 1.35
Nodal line slope (x10)
0.3
0.2
0.1
0.0
-0.1
-0.2
-0.3
-1.0 -0.5 0.0 0.5 1.0
ζ
0.0ps
4.0ps
ω3[10^3 cm^−1] ⟶
ω1[10^4 cm^−1] ⟶